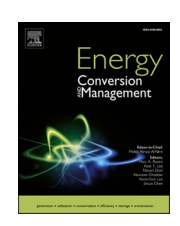
ELSEVIER

Contents lists available at ScienceDirect

## **Energy Conversion and Management**

journal homepage: www.elsevier.com/locate/enconman





# Application relevant load cycles for PEMFC component development and hybrid system optimization

Juan Sanchez-Monreal a,\*, Jens Mitzel o, Christophe Vacquier o, Pawel Gazdzicki

- <sup>a</sup> German Aerospace Center (DLR), Institute of Engineering Thermodynamics, Pfaffenwaldring 38-40, 70569 Stuttgart, Germany
- <sup>b</sup> SYMBIO, 10, rue Specia, 69190 Saint-Fons, France

#### ARTICLE INFO

Keywords:
PEMFC
Load cycling
Heavy-duty
Mission profile
Hybridization strategy
Battery dimensioning
Efficiency

#### ABSTRACT

Polymer electrolyte membrane fuel cells (PEMFCs) are one of the key technologies for the decarbonization of transportation. In contrast to light-duty vehicles (LDV), durability requirements for heavy-duty (HD) transport applications are challenging. To overcome these difficulties, material improvements must be complemented by optimized operation strategies. Furthermore, specific testing protocols in application relevant conditions are required. Harmonized testing protocols already exist for automotive applications. However, for HD applications, such protocols are still pending, which represents a bottleneck for further development. A semi-empirical model is used in a novel systematic top-down methodology to generate application related power demand cycles in PEMFC of an HD hybrid vehicle is presented and demonstrated in detail for the case of PEMFC in HD transport. The resulting load profile, applicable at single cell and stack levels, is proposed as a starting point for a harmonization of open-source HD load cycling and testing protocols for PEMFC component development. Furthermore, the method is also used to evaluate the impact of the energy storage system (ESS) capacity and of the hybridization strategy parameters on the PEMFC stack power demand dynamic and efficiency; providing up to 2 % efficiency increase and a 50 % reduction in FC load changes.

## 1. Introduction

In recent years, polymer exchange membrane fuel cells (PEMFCs) have emerged as a technology in the decarbonization of the transport sector. PEMFC has been implemented commercially in light-duty vehicles (LDV) by a few car manufacturers, but remains in the development stage for heavy-duty vehicles (HDV)[1]. Emissions from HDV applications represent around 25 % [2,3] of total transport related emissions. Therefore, HDVs are becoming the focus of PEMFCs applications. HDV with this technology will benefit from the long range, fast refueling, and high power and energy density that PEMFCs technology offers, particularly for long-haul transport. Typically, this transport type involves tractor-trailer vehicle combinations with a gross vehicle weight (GVW) of about 40 t. High mileage routes (110,000 to 160,000 km a<sup>-1</sup>), with up to 75 % of their mileage in motorways [2], are characteristic.

There are remarkable differences in the targeted Key Performance Indicators (KPIs) between LDV and HDV PEMFC. The durability of PEMFC stacks for HDV must be increased up to 30,000 h, which is 6 times more than the LDV target [4]. On the other hand, power density KPIs have been relaxed but at increased voltages due to the higher

efficiency requirements. The DOE targets to reduce power density from 1.2  $\rm Wcm^{-2}$  for LDV [5] to 0.84  $\rm Wcm^{-2}$  for Class 8 Trailers [6]; FCHJ KPIs reduce the value from 2  $\rm Wcm^{-2}$  @ 0.66 V for LDV [7] to 1.2  $\rm Wcm^{-2}$  @ 0.675 V [4] in HD applications.

PEMFC dynamic response may be slower than required to fulfill the power demand in vehicles, so they are combined into hybrid systems. Energy storage systems (ESS), such as batteries, with faster response are used in combination to cover the high dynamic situations. Different architectures are used in vehicles depending on the requirements [8,9]. Moreover, the strategy followed to split the power (hybridization strategy) shape the power demand to the components [10]. Therefore, it is necessary to understand how a PEMFC delivers power in a HD power train given a certain hybridization strategy. PEMFC testing protocols and driving cycles already exist for automotive in Europe [11], the USA, China, and Japan; but are still missing for HD application at least in the form of a commonly agreed test profile. Chen et al [12] and Nguyen et al. [13] present an extended review of different load cycles for automotive applications. At the moment, there are only very few HD related degradation test protocols available, and they all follow a bottom-up approach at the material level: for membranes [12], for catalysts [13] and for MEA level [13]. To the best of our knowledge, there are no stack

<sup>\*</sup> Corresponding author at: German Aerospace Center (DLR), Institute of Engineering Thermodynamics, Pfaffenwaldring 38-40, 70569 Stuttgart, Germany. E-mail address: Juan.SanchezMonreal@dlr.de (J. Sanchez-Monreal).

Glossary  Acronyms  BoP  BoT	of acronyms and symbols  Balance of plant Beginning of test	$\dot{m}_T \ M_{air} \ M_{O_2} \ M_W \ P_a$	Turbine mass flow [kg s <sup>-1</sup> ] Air molar mass: 0.0289647 kg mol <sup>-1</sup> Oxygen molar mass: 0.0319988 kg mol <sup>-1</sup> Water molar mass: 0.018015 kg mol <sup>-1</sup> Atmospheric pressure [Pa]
Бот ЕоТ	End of test		Cell pressure [Pa]
ESS	Energy storage system	$P_{cell} \ \Delta P_{cell}$	Cell pressure loss [Pa]
FCS	Fuel cell system	$\dot{W}_{elec}$	Electrical power [W]
HD	Heavy duty	$\dot{W}_{C}$	•
HDV	Heavy duty vehicle		Compressor power [W]
MEA	Membrane electrode assembly	$\dot{W}_{ m climb}$	Power required to climb [W]
MoT	Middle of test	$\dot{W}_{ m drag}$	Drag power [W]
	Polymer exchange membrane fuel cell system	$\dot{W}_{ m inertia}$	Inertia power [W]
SD	Shut-down	$\dot{W}_{ m mech}$	Mechanical power [W]
SoC	State of charge	$\dot{W}_{ m rolling}$	Rolling power [W]
SU	Start-up	$\dot{W}_T$	Turbine power [W]
Symbols	•	ν	Vehicle speed [m s <sup>-1</sup> ]
$A_f$	Frontal area [m <sup>2</sup> ]	$V$ $V_{ESS}$	Voltage in power bus [V] Voltage of ESS [V]
а	Acceleration [m s <sup>-1</sup> ]	$V_{FC}$	Voltage of FC [V]
$c_d$	Drag coefficient [-]	$\varepsilon_{DC}$	Efficiency DCDC converter [-]
$c_f$	Friction coefficient [-]	$\varepsilon_{M}$	Efficiency vehicle electrical motor [-]
e F	Rotation factor [-]	$\varepsilon_{PEMFCS}$	Efficiency of PEMFCS [-]
	Faraday constant: $96,485 \text{ C mol}^{-1}$ gravitational acceleration: $9.8 \text{ m s}^{-1}$	$\overline{\varepsilon}_{PEMFCS}$	Average efficiency of the PEMFCS [-]
g I	Current [A]	$\theta$	Road inclination [rad]
$I_{BoP}$	BoP current [A]	$\rho$	Air density: $1.225 \text{ kg m}^{-3}$
$I_{ESS}$	ESS current [A]	$\eta_C$	Isentropic efficiency compressor [-]
I <sub>ESS.HV</sub>	ESS at HV current [A]	$\eta_T$	Isentropic efficiency turbine [-]
$I_{FC}$	Fuel cell current [A]	$\chi_{O_2}$	Oxygen molar fraction in air [-]
$I_{FC.HV}$	FC at HV current [A]	$\lambda_C$	cathode stoichiometry [-]
$I_{N}$	Net PEMFCs current [A]	$\mathbb{E}_{ESS,C}$	Energy charged on the ESS [kWh]
$m_{empty}$	Vehicle empty mass [kg]	$\mathbb{E}_{ESS,D}$	Energy discharged on the ESS [kWh]
$m_{load}$	Vehicle load mass [kg]	$\mathbb{E}_{PEMFCS}$	Net Energy generated by PEMFCS [kWh]
$\dot{m}_C$	Compressor mass flow [kg s <sup>-1</sup> ]	$\mathcal{M}_{H_2}$	Hydrogen stoichiometrically consumed by PEMFCS [kg]

level protocols available nor load cycles derived from a top-down approach considering the driving cycle, the vehicle, or even the hybridization strategy. In this context, it should be noted that the USA consortium Million Mile Fuel Cell Truck M2FCT [2] addresses durability and efficiency challenges in PEMFCs for HD with a focus on long-haul trucks and is also developing test protocols and profiles.

In order to evaluate the lifetime of any vehicle or vehicle component under standardized circumstances, driving cycles are a common approach. A drive cycle must address all the crucial situations in the vehicle's life (rest, start, stop, acceleration, deceleration etc). NREL DriveCAT [14] and the European Commission tool VECTO [15] provide general drive cycles for HDVs which are originally focused on combustion engines, but represent typical transport situations and can be adapted to electric vehicles.

Accelerated tests are necessary to assess lifetime requirements in shorter periods. Several types of these tests are available in literature: accelerated stress tests (AST) [16–18], accelerated degradation tests (ADT) [19] and accelerated lifetime tests (ALT) [20].

The difference between ADT and AST is not always clear in the literature. ASTs are mostly used when the test is addressed to specific stressors [21], while ADTs are used when the test is referred to a specific degradation mechanism [19]. Both are applied to determine the durability of complete stacks or their components [18]. The degradation mechanisms triggered by the applied stressor may not be isolated and depend heavily on the type of test. This category includes the DOE [22] and FCH JU voltage cycling for electrocatalyst and catalyst support degradation, as well as cycling of temperatures or RH for aged

membrane degradation [16]. Ren et al. [23] present a compendium of AST for automotive conditions separated into three FC operating conditions: idling, dynamic load, and start-stop. The authors also included a detailed description of the involved degradation mechanisms, and dynamic load is reported to trigger a broad range of degradation mechanisms. Petrone et al. [21] presented a description of how to design AST and how to avoid new degradation modes not already present in normal operation.

ALT is another type of test in which degradation is accelerated by adapting nominal operation conditions, e.g. by increasing temperatures, pressures, or loads without focusing on isolation of individual degradation mechanisms [20,24]. All possible degradation processes expected during the life-time are involved in the same test, which makes it more difficult to analyze the impact of individual stressors or the effect on one single component. However, ALT enables realistic estimation of fuel cell lifetime in shortened test duration. In this context it is particularly important to take into account the superposition of reversible and irreversible performance losses [25,26] by applying appropriate recovery procedures [27,28]. ALT are mainly used to determine system, stack, or MEA lifetime without in-depth analysis of involved processes. Table S1 in Supporting Information contains a comparison between AST, ADT and ALT.

Several available approaches to develop AST, ADT, and ALT are reported [19–21,24,29]. All of them require, as a first step, a clear identification of the power demand and the stressors involved in the expected degradation scenario. Chen et al. [12] reviewed durability test protocols based on driving cycles for LDV and city buses. Recently,

Thiele et al. used the PEMFC current profile measured in a FCEV tested in a chassis dynamometer following a LDV driving cycle [30] and extract the degradation relevant parts of the cycle [31]. Colombo et al. [32] applied automotive specific start-up AST [33] and benchmarked it against standard DOE AST [22]. Lately Mora et al. [34] also evaluated automotive representative AST [35] obtained from real drive data. It is very important that the applied driving cycle and conditions fit the desired critical conditions of the specific vehicle application and there is a clear lack of HD-specific driving cycles at the moment.

In this work, a novel systematic methodology to generate application related power demand cycles in a PEMFC of a HD hybrid vehicle is presented and demonstrated in detail for the HD transport case. The method commences with a mechanical model to estimate power demand from driving cycles. Secondly, a semi-empirical model for PEMFC-based hybrid systems is introduced, as well as a hybridization strategy to split the power demand between PEMFC and ESS. Then, the models are used to estimate the behavior of a specific system in a defined driving cycle. The application case of a generic tractor-trailer with GVW up to 40 t during a representative driving day, including necessary mandatory rest periods, is presented. Since application related load cycles are crucial to develop specific fuel cell systems and to optimize their components, lifetime tests require harmonization and standardization. Therefore, the presented PEMFC load cycle can be used as a HD application representative cycle for tests in single cells and in stacks to mitigate the lack of such test procedures. Consequently, the resulting cycle can be considered as a starting point for a harmonized, open-source HD load cycle for PEMFC component development and further development of ALT for HD application. In addition, the presented methodology is systematically applied to the study of the influence of the ESS capacity and the hybridization strategy on the resulting power demand of the PEMFC system, and how hybrid system design and hybridization strategy can influence their efficiency and lifetime.

## 2. Methodology

A scheme of the calculation workflow is presented in Fig. 1. The proposed methodology obtains the power demand in the PEM fuel cell system (PEMFCS) from the calculated mechanical power demand required for a given vehicle to fulfill a representative driving cycle. The hybridization strategy is used to split the power between the PEMFCS and the ESS. A simplified model of the PEMFCS is used to obtain the net power production and the BoP power consumption.

#### 2.1. Mechanical model

Power demand profiles can be obtained from driving cycles, which are defined in terms of vehicle speed and road gradient versus time.

Assuming the mass and the size of the vehicle, the required power to maintain the speed can be calculated. The resulting dynamic load profile includes typically sharp increases and decreases in the power demand. The required mechanical power is expressed as the sum of inertial  $\dot{W}_{inertia}$ , climb  $\dot{W}_{climb}$ , rolling  $\dot{W}_{rolling}$ , and aerodynamic drag  $\dot{W}_{drag}$  powers [36], and are calculated according to Appendix A. A detailed derivation of this model is presented by Echard et al. [36]. Positive mechanical power obtained from this cycle analysis is used as the power demand of the electrical motor, including the efficiency of the electrical motor  $\epsilon_M$  (Appendix A). The negative mechanical power indicates that the vehicle is braking, and therefore is accounted for as available kinetic recoverable power. However, for simplicity, recuperation of kinetic energy is not considered in this work. The output of this mechanical model is therefore the net power demand of the electric motor in a hybrid electric HD truck.

## 2.2. Electrical power and hybrid system

The electrical power to the motor must be supplied by the hybrid combination of the PEMFCS and ESS. A typical layout of the electric power system [8] is presented in Fig. 2. The power demand on the system is translated into a current demand in the high-voltage (HV) line with fixed voltage. The main task of the converters is to homogenize the power output of the PEMFCS and the ESS to the HV line. While the converter connected to the PEMFCS operates only in one way, from low voltage (LV) of the PEMFCS to the HV line (boost operation), the converter of the ESS must operate in both directions, for example, from ESS to HV line (boost) and HV line to ESS (buck mode). The buck mode is used to recharge the ESS with the line power excess.

A semi-empirical energetic model is used to determine the operative conditions of all the components of the hybrid system; equations of the model are presented in Appendix A. The HV current distribution is calculated based on electric energy balances between the components. Operative points at the LV-side of the PEMFCS and the ESS are determined using experimental polarization curves. DCDC converters are considered to provide the voltage transformation with a power loss modeled by an efficiency factor (92 %).

In addition, it is necessary to include a hybrid strategy to quantitatively determine the power distribution. This strategy is crucial and can drastically change the power demand on PEMFCS and ESS depending on the overall goal. The hybrid strategy ambition can vary in goals and complexity: optimizing efficiencies (global or PEMFCS or ESS, etc.) [37], protecting components by avoiding damaging operation conditions, reducing the dynamic load to the PEMFCS, but also keeping a certain state of charge (SoC) in the ESS for efficiency and lifetime optimization, or simply as a power reserve for steep road sections. Several strategies

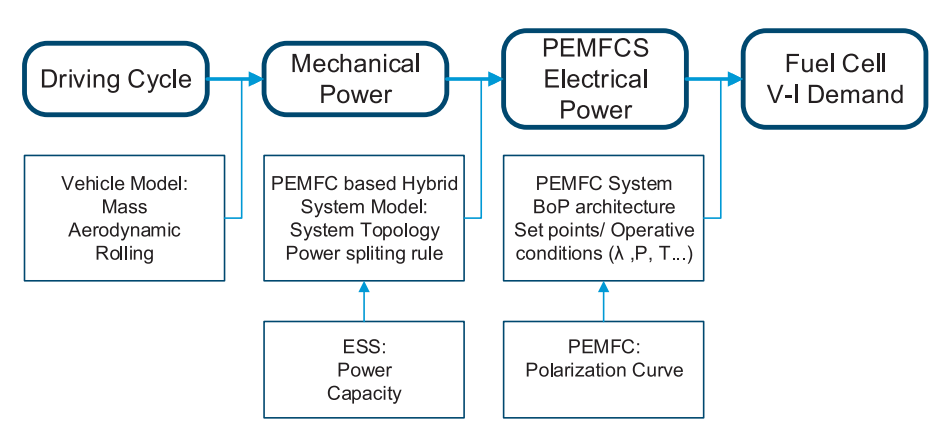


Fig. 1. Flow diagram of calculation methodology. From driving cycles and a vehicle model, mechanical power is calculated. Later, it is combined with a PEMFC based hybrid model (including ESS properties) to obtain the electrical power demanded to the PEMFCS. Afterwards, using a PEMFCS model (including BoP and FC properties) the V-I FC demand is calculated.

Fig. 2. Scheme of the hybrid system layout, (a) flow of electrical power in the PEMFCS + ESS hybrid system and (b) architecture of the PEMFCS.

are proposed in the literature [9,36,38,39,40,41]. In this work, a rule-based strategy is used.

The power splitting between PEMFCS and ESS is based on the SoC of the ESS. The PEMFCS is operated in discrete current levels that progressively increase the power output following the ESS discharge. The minimum PEMFCS power level is high enough to avoid OCV and related degradation. The use of discrete operative points instead of continuous load range operation simplifies the optimization of the operation. Since the SoC varies slowly, the PEMFCS power output continuously changes in controlled steps, for example, it moves only one current level up or down, avoiding large load steps at high gradients. A dead-band of 0.2 % SoC between zones is used to prevent unnecessary oscillations around the thresholds. The equations of the model are summarized in Appendix A.

Even if this strategy is simple, the selection of the SoC thresholds and PEMFCS power levels can shape different behaviors. A narrow amplitude between SoC thresholds leads to the holding of a minimum SoC as reserve, while a broader amplitude forces the use of the available energy in the ESS. Moreover, the finite amount of discrete operation points of the PEMFC favors the optimization of the BoP strategy and its components.

In order to analyze the results of the model for different cases, some global and average magnitudes can be calculated, namely, energy produced by PEMFCS ( $\mathbb{E}_{PEMFCS}$ ), energies charged and discharged on the ESS ( $\mathbb{E}_{ESS,C}$  and  $\mathbb{E}_{ESS,D}$ ).

## 2.3. PEMFCS

Polarization curves from experiments are used to model the voltagecurrent behavior of the stack at different pressures, temperatures, and humidity. The architecture of the PEMFCS is shown in Fig. 2 (b). The cathode side of the PEMFCS is depicted with an inlet compressor and an exhaust turbine to recover power from expansion residual gases. The power required for the cathode compressor and recovered by the turbine is calculated from the cathode mass flow and isentropic efficiencies [42]. Cathode stoichiometry is mapped for different current densities; isentropic efficiencies are mapped for different mass flows.

As a simplification, the required total BoP power input is calculated as a 110 % factor of the compressor power input to consider the consumption of the rest of the components not modeled (i.e., recirculation pump, coolant pump, valves, ...). The net power of the PEMFCS is then calculated as the power generated by the stack minus the required total BoP power. Humidification and temperature control are not included in this simplified model.

In order to better understand and compare the results for different cases, global magnitudes have to be computed for the PEMFCS also. Particularly, hydrogen consumed stoichiometrically ( $\mathcal{M}_{H_2}$ ) and average efficiency of the PEMFCS ( $\overline{\epsilon}_{PEMFCS}$ ) can be calculated.

## 3. Application case

The aim of this work is to provide an HD long-haul relevant PEMFC load cycle for accelerated durability tests in single cells and in stacks. The vehicle selected for this purpose is a generic tractor trailer with GVW up to 40 t. Model parameters of the vehicle are summarized in Table 1 The used driving cycle represents a driving day of 11 h 45 min, including stops. It is a combination of the VECTO long-haul and urban cycles to represent pickup, transport, and delivery. The stops are included to represent vehicle payload load, but also the driver's mandatory pauses. Speed and climbing grade are presented in Fig. 5.

The PEMFCS defined for this application case (Fig. 2b) is based on the M2FCT reference fuel cell system [2] for heavy-duty trucks whose PEMFCS provides 275 kW electric power. Following the suggestion of the M2FCT, the system is composed of 4 stacks in parallel. Each stack has a 300 cm² active area and 275 cells. The air supply is provided by a single turbo-compressor. An expansion turbine is included to recover power from cathode exhaust gases. Parameters used for the PEMFCS are provided in Table 2.

The stack voltage-current performances are obtained from scaling up a single-cell polarization curve from a commercial MEA obtained in our lab to the considered active area and number of cells. Fig. 3 presents the polarization curve data as well as the resulting net polarization curve for the considered BoP. The Figure also contains the stoichiometry of the cathode as well as the isentropic efficiency maps of the compressor and turbine used in the air supply system.

In this first application case, and in contrast to the M2FCT system (using 70 kWh), a battery with 150 kWh capacity is used as ESS. Although the cycle can be fulfilled with a smaller capacity (see section 3.2), a larger capacity allows a reserve capacity to address in every moment more than 35 min at 400 kW (i.e. 6 % climb at 50 kmh $^{-1}$  for 35 min). To this end, the hybridization strategy is focused on maintaining the SoC over 60 %. Additionally, this keeps the battery in the efficient range at SoCs over 55 % [45]. To that end, a narrow set of zones around the desired SoC (blue box in Fig. 4) is used. Table 2 presents a summary of the PEMFCS parameters used.

The power demand calculated to fulfill the cycle is presented in Fig. 5. Time in power zones of PEMFCS, ESS, and demand is presented in Fig. 7. (Supporting information encompasses Table S2 with the same information, but numerically). Fig. 7 also presents the changes between power zones of the PEMFCS. The system fulfills the power demand

 Table 1

 Vehicle parameters (VECTO Class 5 Tractor [15]).

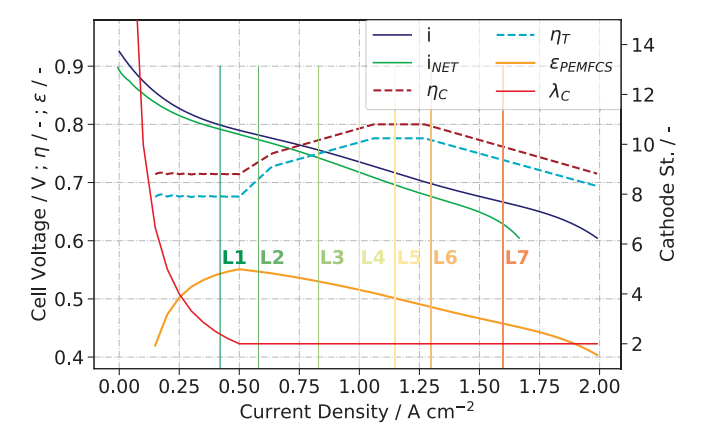
venicle parameters (VEGTO class 3 Tractor [15]).				
GVW	35029 kg			
Vehicle	15729 kg			
Load	19300 kg			
Frontal area $\times$ C <sub>d</sub>	$5.3 \text{ m}^2$			
$C_{r}$	0.006			
Rolling part inertial coefficient	1.05			

Table 2
PEMFCS and ESS parameters.

PEMFC Parameters				
Number of cells [2]	275			
Number of stacks [2]	4			
Active area [2]	300 cm <sup>2</sup>			
Max current	750 A (1.66 A cm <sup>-2</sup> )			
Cathode stoichiometry	$2.0 \text{ for i} > 0.5 \text{ A cm}^{-2}$			
Absolute pressure (stack outlet) [2]	2.5 bar			
Temperature (stack inlet) [2]	90 °C			
BoP and auxiliary				
Isentropic efficiency compressor [42]	0.7—0.8			
Isentropic efficiency turbine [42]	0.7—0.8			
Motor electrical efficiency $\varepsilon_M$ [36]	0.9			
DCDC converter efficiency $\varepsilon_{DC}$ [43]	0.92			
BoP power [44]	$110~\%\dot{W}_C$			
ESS parameters				
Capacity	35, 70 & <b>150</b> <sup>a</sup> kWh			
Initial SoC	0.6a (narrow SoC thresholds)b			
	0.88 (broad SoC thresholds)			
Max. SoC range	2–98 %			

<sup>&</sup>lt;sup>a</sup> Reference case.

<sup>&</sup>lt;sup>b</sup> Compare Fig. 4.



**Fig. 3.** Experimentally obtained polarization curve used for stack cell, compressor and turbine efficiency, and PEMFCS efficiency (left axis), and cathode stoichiometry used (right axis). Compressor and turbine efficiencies are calculated with the mass flow required at the corresponding current density. Colored vertical lines indicate the discrete operation PEMFCS current levels (L1 to L7, compare Fig. 4) corresponding to the seven (Z1 to Z7) SoC zones.

without any gap and always maintains an ESS SoC of  $\sim 60$ % for energy reserve. Load and discharge of the ESS, as a result, happen mainly in the same range of SoC. The system spends 23 % of the cycle idle and more than 50 % below 35 % of the maximum power of the PEMFC. The PEMFCS does not reach zone 7. A greater number of power zone changes occur between levels 1, 2, and 3 (71 % of up & down changes). The resulting load cycle of this application case can be considered as a standard HD load cycle, which is used in different EU projects (PEMTASTIC, RealHyFC). This cycle can be a starting point for a harmonized, open-source HD load cycle for PEMFC component development and is available in the supplementary data.

In addition to the presented application case, the experimental demonstration of the proposed cycle for HD application (section 3.1) and two sensitivity studies related to ESS size (section 3.2) and SoC threshold levels (section 3.3) were performed.

#### 3.1. HD relevant PEMFC load cycle

From the previously obtained power splitting in the hybrid system, the cell voltage and current density in the stack cells are also obtained. Fig. 5 presents the resulting profiles for the studied case. Especially, the cell voltage profile can be used as a representative HD test profile for development and optimization of MEAs in differential single cells. Specific positions in a typical PEMFC stack for HD application can be mimicked by applying the relevant operating conditions (Fig. 6a) and the developed cell voltage profile. Such a test was used for the evaluation of occurring degradation processes in a MEA during 1500 h of operation. The resulting current density in two consecutive cycles is shown in Fig. 6b. As discussed, this cycle includes several stop phases without fuel cell operation dedicated to loading goods and required breaks for the driver. These phases can have a major impact on the degradation behavior, and start-up (SU) and shut-down (SD) procedures have to be precisely defined to enable reliable evaluation of degradation processes during HD operation. Typically, short stops (<30 min) do not include cell cool-down, while long stops do.

For HD application-specific assessment in a laboratory, the use of nitrogen for electrode inertisation should be avoided during both phases. This can result in the non-representative aspect that the open circuit cell voltage remains high during the stop. As a consequence, the cathode potential could be above 0.8 V, resulting in substantial degradation. This phenomenon is shown in Fig. 6c for the original setup (red line), and there are different possibilities to lower the cell voltage in stop phases. Maintaining the hydrogen flow at the anode (blue line) in Fig. 6c should enable hydrogen crossover to the cathode and consumption of the oxygen, resulting in decreased cell voltage. However, the experimental setup has shown that oxygen can permeate from the test bench to the cell, and the resulting OCV is still too high and irreproducible. An additional one-way valve in the air outlet (green line) does not successfully avoid this permeation. Oxygen still seems to enter the cell. Only the use of two shut-down valves in the air inlet and outlet (orange line) in Fig. 6c, resulted in fast and reproducible lowering of the cell potential and is considered to be the best method for degradation studies with cell conditions as close as possible to the HD application. Another option would be the continuous consumption of entering oxygen by the electronic load of the test bench by applying a constant voltage set point of 0.2 V (purple line). This method enables the quantification of the oxygen amount entering the cell during the stop phase by integration of the resulting current. In the presented test, only 2 mL of oxygen was detected to cause the remaining high potential in the original setup.

Exemplarily, the presented test was used to evaluate the impact of 1500 h of HD operation on a specific catalyst (Fig. 6d). Therefore, the electrochemically active surface was determined at the beginning-of-test (BoT), mid-of-test after 500 h (MoT), and end-of-test after 1500 h (EoT) by analyzing the hydrogen adsorption charge between 0.4 and 0.07 V using cyclic voltammetry [46]. This surface is a measure of the catalyst activity, and it could be shown that the used catalyst loses about 30 % mostly during the first 500 h.

## 3.2. Effect of ESS size

The size of the ESS has a direct influence on the PEMFCS power demand. In order to study the effect, simulations with two smaller capacities of the ESS are performed, namely 70 kWh and 35 kWh. The reduction of ESS capacity diminishes the reserve time of the vehicle to deliver 400 kW at any moment. The reserve time is therefore reduced to 14 min and 7 min, respectively. The threshold levels are set in terms of percentual SoC, which is relative to the ESS absolute capacity, so a change in ESS size will therefore modify the absolute energy between the threshold levels. Besides non-linear effects, 1 % of SoC represents approximately 1.5 kWh, 0.7 kWh, and 0.35 kWh of energy, respectively, for each ESS considered size. A reduction of the size of the ESS will lead to a faster change of the percentual SoC for the same power input/

<sup>&</sup>lt;sup>1</sup> PEMTASTIC G.A.: 101101433; RealHyFC G.A.: 101111904.

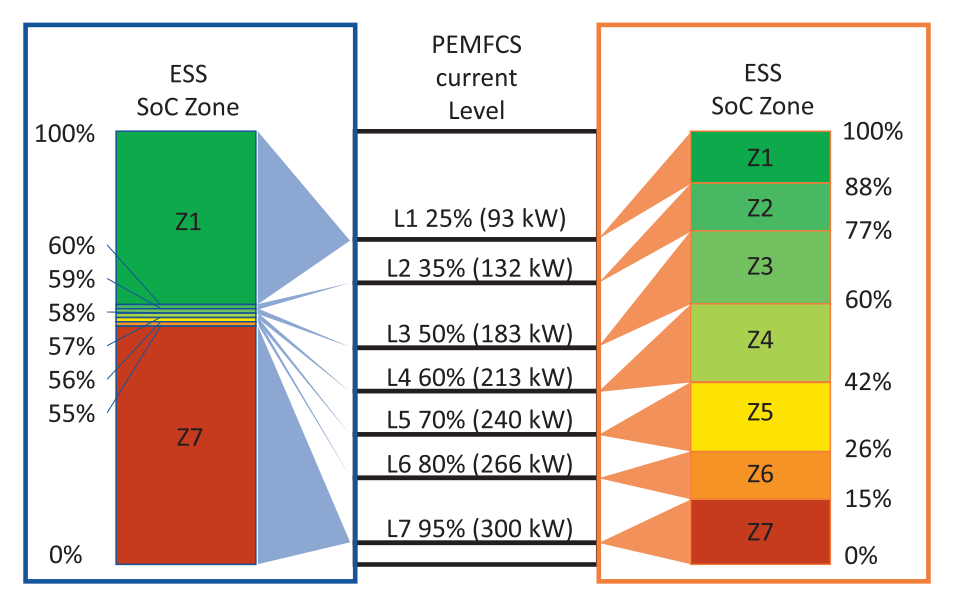


Fig. 4. Hybridization strategies for PEMFCS in discrete levels based in ESS SoC. In brackets approximate net power produced by the PEMFCS. Blue box, narrow thresholds SoC levels between 55% and 60%. Orange box, full range of SoC threshold levels.

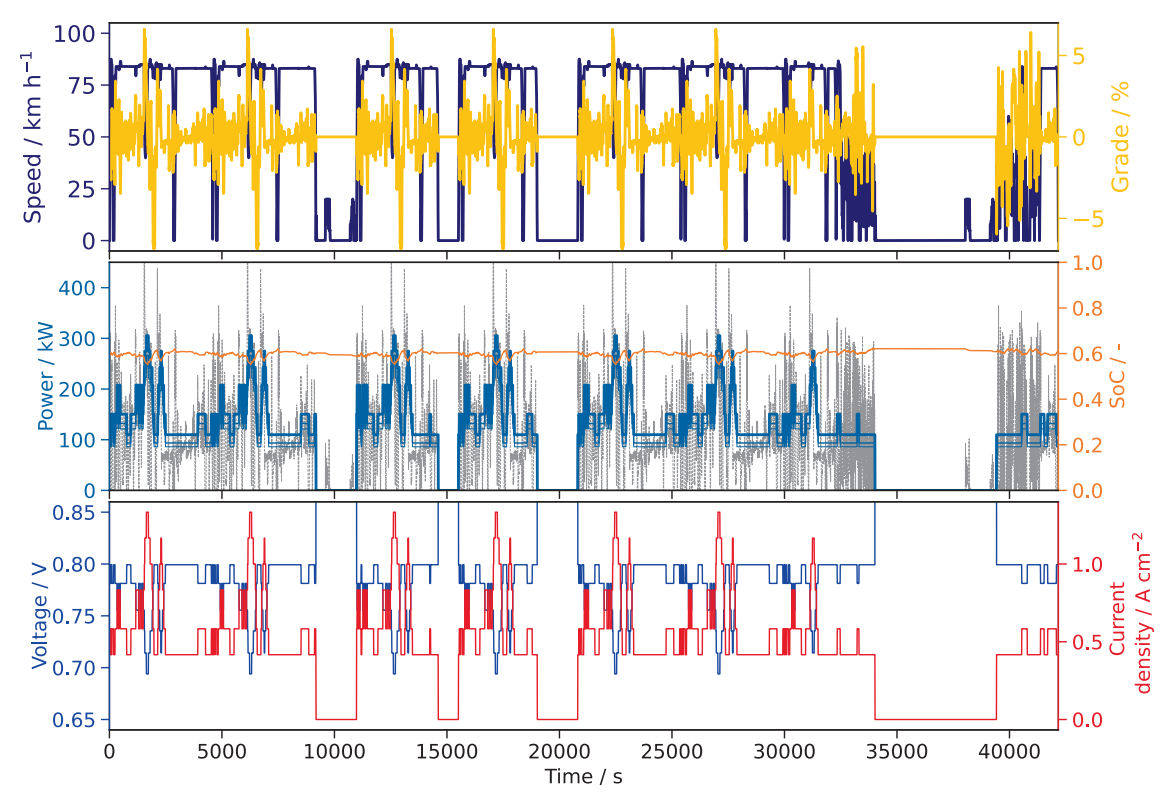


Fig. 5. Up: Driving cycle used. Speed and inclination grade are presented along the cycle duration. Middle: Power demand (grey), power produced by the PEMFCS (Thick blue for stack power, thin blue for PEMFCS power and power after DCDC converter) together with the SoC of the Battery for the analyzed cycle. Bottom: cell voltage and current density in the stack.

## output.

Fig. 7 presents the time in power zones of the PEMFCS for different ESS sizes: 150 kWh, 70 kWh, and 35 kWh. The number of up changes between power levels is also accounted for. Fig. 7 also depicts the energy produced, hydrogen consumed, and efficiency of the PEMFCS. For smaller ESS capacities, the time in zone 1 (25 % of PEMFCS power and highest efficiency) increases, as well as time in zone 7 (95 % of PEMFCS power and lowest efficiency) at the expense of time in zones 2 & 3 mainly. The power produced by the PEMFCS leads to an alternation

between the lowest and highest zones, and the ESS SoC travels through all the threshold levels several times. The number of changes between the power zones increases by almost 80 % in the case of an ESS of 70 kWh and doubles for an ESS of 35 kWh. Detailed tables and graphs are presented in the supporting information (Table S2 & Fig. S2).

The increase in time on the highest zones directly impacts the resultant efficiency of the PEMFCS. The ESS of 35 kWh capacity consumes about 1 kg extra; however, less energy is generated. This indicates a clear decrease in the efficiency of the PEMFCS. It can be noticed that a

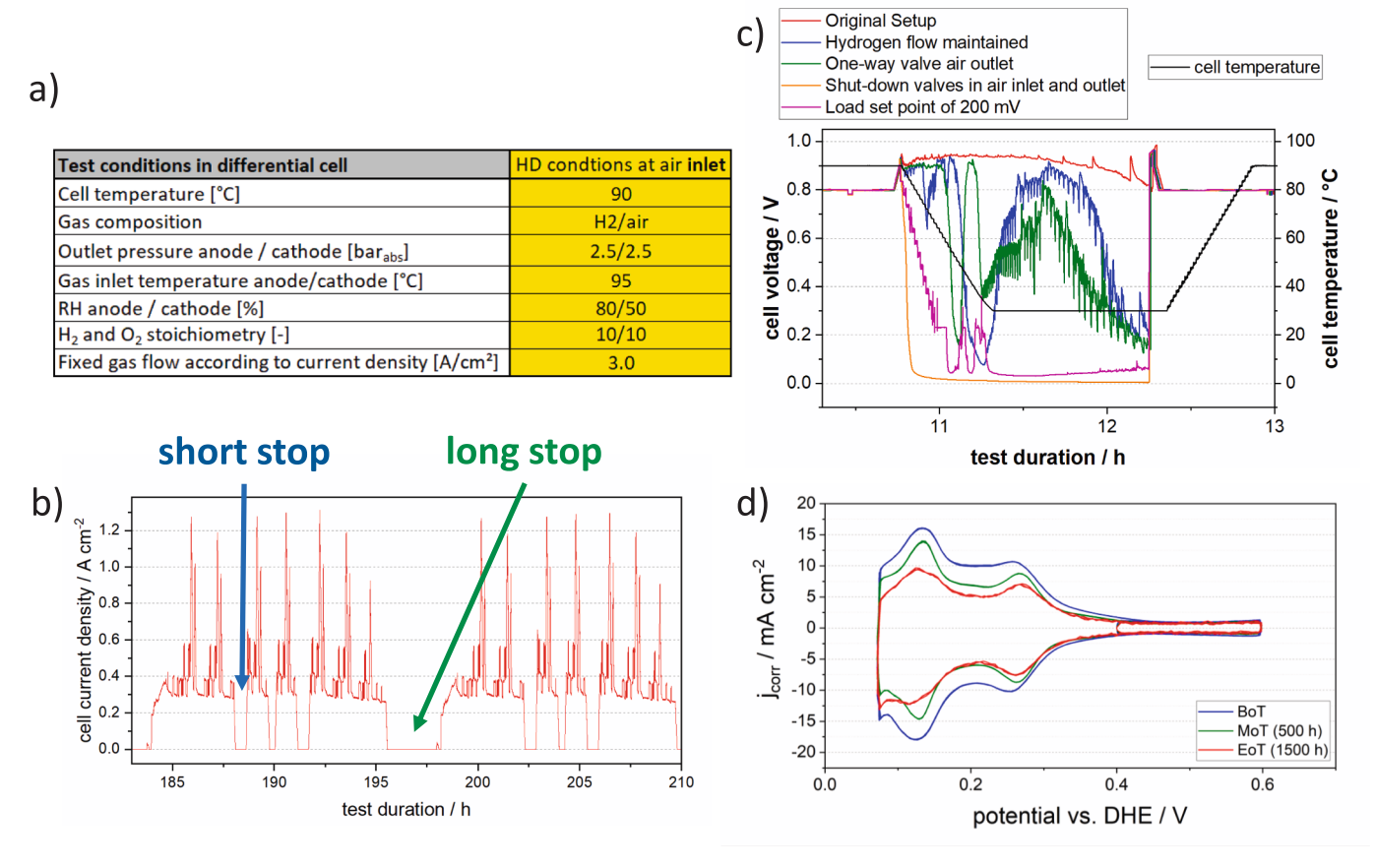


Fig. 6. Example regarding MEA development for HD application by a 1500 h durability test. (a) Applied HD relevant operating conditions, (b) resulting current density profile during the test, (c) impact of setup on cell voltage during stop phases, and (d) impact of durability test on active catalyst surface.

larger ESS capacity induces a behavior of the PEMFCS similar to a range extender. The resulting lower dynamic of the PEMFCS and the operation at lower power zones result in higher efficiency, lower hydrogen consumption, and increased vehicle range. On the other hand, a smaller ESS capacity leads to a more dynamic actuation of the PEMFCS (Fig. 7b) in parallel to a reduction of efficiency (Fig. 7c).

In Fig. 7 the energy charged and discharged on the ESS is also displayed. It can be observed that there is a slightly clear balance between charge and discharge in the ESS. This fact may be a good indication that ESS acts as a buffer of energy, covering appropriately the over- and/or underproductions of the PEMFCS.

## 3.3. Effect of SoC threshold levels

For the three previous cases of ESS size, an additional simulation was carried out, allowing a broader SoC range of the ESS without special attention to reserve time of the vehicle to deliver 400 kW, and enlarging the gap between SoC threshold levels from 1 % up to 11 %. This change leads to an increase in the energy between zone changes to 16.5 kWh, 7.7 kWh, and 3.85 kWh for ESS capacities of 150 kW, 70 kW, and 35 kW, respectively. Maintaining ESS capacity but enlarging the percentual SoC threshold levels also has a direct influence on the time in power zones and the changes between them. The energy required to drop or rise from one zone to another is increased. As a result, for the same power demand, the time in a specific power zone increases, and the number of changes decreases. The initial SoC of the ESS is set to 88 % in order to start the simulation at the same PEMFCS power level (25 %) as in the previous cases.

Fig. 7 summarizes the time in the different power levels of the PEMFCS as well as the up changes between levels. Fig. 7 also presents the energy produced, hydrogen consumed, and efficiency of the

PEMFCS. It can be observed that the most frequently used power level using the broad SoC range is zone 2, compared to zone 1 for the narrow SoC range. This indicates that the PEMFCS operates at higher power at the expense of the stored energy in the ESS. Additionally, the hybridization strategy using a broader SoC range minimizes the PEMFC operation in the power levels 5–7. Detailed tables and graphs of each case are presented in the supporting information (Table S3 & Fig. S2).

In terms of hydrogen consumption, the behavior is similar to the case with narrow thresholds, but the differences for the varied ESS capacities are much smaller in comparison. Nevertheless, the case with the largest ESS capacity consumes less hydrogen and operates the PEMFCS more efficiently. Compared to the case of narrow zones, the PEMFCS generates a similar amount of energy but consumes circa 1 kg of hydrogen less. This demonstrates that the PEMFCS operates at higher efficiency. It can be observed that there is also a similarity between the energy charged and discharged in the ESS, which indicates that the ESS plays the role of an energy buffer. However, for this case, the charged/discharged energy increases significantly (35, 41, and 45 kWh more), which indicates a higher amount of rearranged energy. The broader range of SoC threshold results in a significant reduction in the number of level changes for the PEMFCS and increases the rearranged energy by the ESS. It can be expected that this less dynamic operation of the PEMFCS is beneficial for the PEMFCS lifetime [23].

Fig. 8a and Fig. 8b present a comparison between the cases with 150 kWh ESS capacity. It is remarkable that the SoC of the ESS oscillates around different levels (60 % for the narrow case and 88 % for the broad case). Nevertheless, the value corresponds with the same power levels of the PEMFCS, power level 1 and 2. It has to be noted that the total electrical energy demanded is 1018 kWh, this demand is spread over 475 min of the 705 min, which leads to an average power demand of about 129 kWh. Power levels 1 and 2 are under and over this value



Fig. 7. a) PEMFCS time fraction in power levels. b) number of up-changes between power zones within the cycle. c) Energy produced, hydrogen consumption and efficiency of the PEMFCS and energy charged and discharged of the ESS. Presented for the three ESS capacities studied. Blue box indicates narrow SoC threshold levels, orange box indicates broader range of SoC thresholds levels (corresponding color with Fig. 4).

(Fig. 4). Consequently, the selection of the SoC zones corresponding to the power levels around the average power demand is crucial because the SoC will oscillate mainly in that range. Moreover, SoC oscillation amplitude is clearly different between the presented cases. For narrow zones, the SoC moves between 60 % and 56 % meanwhile, for the broad zones, this variation occurs between 89 % and 76 %. Fig. 8c presents the case of an ESS capacity of 35 kWh and broad zones, where the SoC falls to 54 %. Thus, the SoC window during operation depends strongly on the hybridization strategy and the ESS capacity. To minimize complexity ESS charge/discharge efficiency [45] has not been considered for this work, but could be included in the future. Nevertheless, the presented outcome can be used to adapt the PEMFCS levels to the most efficient range of ESS SoC; in terms of value and range of oscillation.

## 4. Conclusion and outlook

A novel top-down methodology to generate PEMFC representative power profiles is presented and employed to analyze a representative case of HD long-haul truck closing the gap regarding the lack of

representative cycles or testing protocols for this case. Nevertheless, the presented methodology can be directly applied to other road and off-road vehicles like buses, forklifts as well as other industrial vehicles that require harmonized application of relevant load cycles. In addition, this method includes the possibility of using different hybridization strategies. Consequently, if a power demand profile for any given application is available, the presented methodology can be used to derive the application-relevant PEMFCS power profile.

Based on the performance data of the MEAs implemented in the used PEMFC stack, this methodology also enables the break-down of various application cases consisting of current density and voltage profiles in the dedicated single cells. A direct application of this approach is also depicted in this work. The voltage profile obtained for a relevant HD application has been used in a differential cell to study the degradation behavior of MEAs and the impact of applied start-up and shut-down procedures. The presented load cycle of this application case can be considered as a standard HD load cycle and, most importantly, a starting point for a harmonized, open-source HD load cycle for PEMFC component development (available in the supplementary data). In the future,

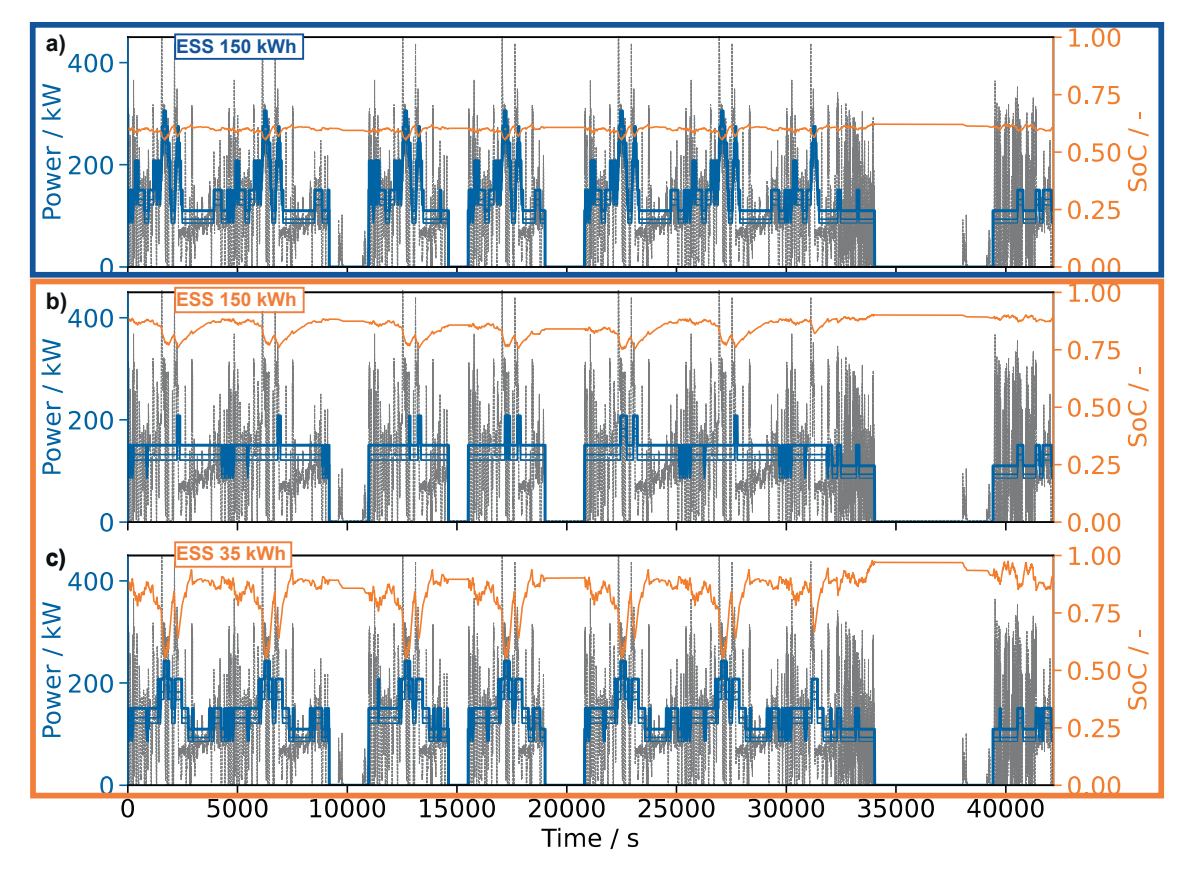


**Fig. 8.** Comparison of PEMFCS power, Power demand (grey), and ESS SoC between: a) 150 kWh narrow SoC thresholds and initial SoC = 60 % (blue box); b) 150 kWh broad zones and initial SoC = 88 % (orange box) and c) 35 kWh broad zones and initial SoC = 88 % (orange box). It is noted that the oscillations in the case of broad zones exhibit larger amplitude.

the degradations observed after applying the accelerated cycle have to be analyzed in relation to specific sequences, which will provide insights into the development of specific accelerated cycles.

The hybridization strategy has a dramatic impact on PEMFCS demand and, consequently, on PEMFC stack operation conditions. Hybridization strategy directly impacts the dynamic load cycling of the PEMFC stack, which creates dynamic thermal, humidity, reactant demand, and potential cycling [23], which is known to be the main contributor to PEMFC degradation [47]. In this work, a hybridization strategy is proposed based on operating the PEMFCS in discrete operation levels in correlation with SoC zones of the ESS. The strategy is entirely independent of the type of ESS employed. The studied strategy simplifies the operation of the PEMFCS but can also improve the possibility of the ESS acting as a beneficial energy buffer system. A large ESS capacity leads to more efficient operation of the PEMFCS due to increased operation at medium current densities and therefore higher cell voltages. This operation allows lower operating temperatures that extend the durability of electrodes and membranes [2]. A smaller ESS capacity induces an increase in PEMFCS operation at higher current densities and therefore lower efficiencies. Furthermore, an increase in changes between operation points of the PEMFCS might decrease its lifetime. A narrow set of ESS SoC threshold levels assures an energy reserve for unexpected power demands but also shows a more constant SoC of ESS and a more dynamic operation of the PEMFCS. A broader set of ESS SoC thresholds shows an increase in efficiency by 2 % and a more stable operation of the PEMFCS (50 % less power level changes), but a wider oscillation in ESS. Consequently, the selection of the SoC threshold corresponding to the power levels under and above the average power demand arises as crucial due to the ESS SoC oscillating around this value. Therefore, it can be selected to maintain the ESS at an

efficient and reliable value. To that end, this model may be combined with a more detailed ESS model considering non-constant charge/discharge efficiencies of the ESS.

## CRediT authorship contribution statement

Juan Sanchez-Monreal: Writing – review & editing, Writing – original draft, Visualization, Software, Methodology, Conceptualization. Jens Mitzel: Writing – review & editing, Visualization, Investigation, Conceptualization. Christophe Vacquier: Writing – review & editing, Project administration, Funding acquisition.

## Declaration of competing interest

The authors declare the following financial interests/personal relationships which may be considered as potential competing interests: Juan Sanchez-Monreal, Jens Mitzel, Christophe Vacquier, Pawel Gazdzicki, reports financial support was provided by Clean Hydrogen Partnership and is members Hydrogen Europe and Hydrogen Europe Research (Project 101101433 PEMTASTIC). If there are other authors, they declare that they have no known competing financial interests or personal relationships that could have appeared to influence the work reported in this paper.

## Acknowledgments

This project is supported by the Clean Hydrogen Partnership and its members Hydrogen Europe and Hydrogen Europe Research (Project 101101433 PEMTASTIC).

## Appendix A

#### Model equations

Mechanical power [36]	$\dot{W}_{ m mech} = \dot{W}_{ m inertia} + \dot{W}_{ m climb} + \dot{W}_{ m rolling} + \dot{W}_{ m drag}$
Power required due to inertia [36]	$\dot{W}_{inertia} = (e \bullet m_{empty} + m_{payload}) \bullet a \bullet v$
Power required to climb [36]	$\dot{W}_{\text{climb}} = (m_{\text{empty}} + m_{\text{payload}}) \bullet g \bullet \sin(\theta) \bullet v$
Rolling power [36]	$\dot{W}_{rolling} = (m_{empty} + m_{payload}) \bullet g \bullet c_f \bullet v$
Electrical power [36]	$\dot{W}_{elec} = \dot{W}_{ m mech}^{+}/arepsilon_{M}$
Drag power [36]	$\dot{W}_{drag} = \frac{1}{2} \rho \bullet c_D \bullet A_f \bullet v^3$
Bidirectional DCDC converter [43]	Discharge: $\varepsilon_{DC} I_{ESS} \bullet V_{ESS} = I_{ESS,HV} \bullet V$
	Charge: $I_{ESS} \bullet V_{ESS} = \varepsilon_{DC} I_{ESS,HV} \bullet V$
FC converter [43]	$arepsilon_{DC}I_{ ext{FC}}ulletV_{ ext{FC}}(I_{FC})=I_{ ext{FC}, ext{HV}}ulletV$
Current at HV level	$I_{HV} = I_{FC,HV} + I_{ESS,HV}$
Polarization curve	I(V) Experimentally obtained
PEMFCS Net current [44]	$I_{FC} = I(V) - I_{BoP}(I)$ (implicit solver for $I$ )
BoP current bleed [44]	$I_{BoP} = \left(1.1 \dot{W}_C + \dot{W}_T\right)/V$
Compressor [42]	$\dot{W}_C = rac{c_p T_a}{\eta_C} \left( \left(rac{P_{cell} + \Delta P_{cell}}{P_a} ight)^{\gamma-1/\gamma} - 1  ight) \dot{m}_C$
Turbine [42]	$\dot{W}_T = c_p T_{cell} \eta_T \Biggl( \Biggl( rac{P_a}{P_{cell}} \Biggr)^{\gamma - 1/\gamma} - 1 \Biggr) \dot{m}_T$
Mass flow compressor [48]	$\dot{m}_C = n_{cells} rac{I}{4F} rac{1}{\chi_{O_2}} M_{air} \lambda_C$
Mass flow turbine [48]	$\dot{m}_T = \dot{m}_C + rac{I}{4F}(2M_W - M_{O_2})$
Efficiency PEMFCS [48]	$arepsilon_{PEMFCS} = rac{I_{FC} ullet V}{LHV_{H_2} ullet I/2F}$
Energy charged/discharged on the ESS	$\mathbb{E}_{ESS,C} = \int_0^{t_{end}} V \bullet I_{ESS,HV}^+ \mathrm{dt}; \mathbb{E}_{ESS,D} = \int_0^{t_{end}} V \bullet I_{ESS,HV}^- \mathrm{dt}$
Energy generated by PEMFCS	$\mathbb{E}_{PEMFCS} = \int_0^{t_{end}} V_{FC} \bullet I_{FC} dt$
Hydrogen stoichiometrically consumed by PEMFCS	$\mathcal{M}_{H_2} = \int_0^{t_{end}} n_{cells} \frac{I}{2F} M_{H_2} dt$
Average efficiency of the PEMFCS	$\overline{\varepsilon}_{PEMFCS} = \mathbb{E}_{PEMFCS} / \mathscr{M}_{H_2} \bullet LHV_{H_2}$

## Appendix A. Supplementary data

Supplementary data to this article can be found online at https://doi.org/10.1016/j.enconman.2025.120604.

#### Data availability

Data will be made available on request.

## References

- [1] Mancino A, Menale C, Vellucci F, Pasquali M, Bubbico R. PEM fuel Cell applications in Road Transport. Energies 2023;16(17). https://doi.org/10.3390/en16176129.
- [2] Cullen DA, Neyerlin KC, Ahluwalia RK, Mukundan R, More KL, Borup RL, et al. New roads and challenges for fuel cells in heavy-duty transportation. Nat Energy 2021; 6(5):462–74. https://doi.org/10.1038/s41560-021-00775-z.
- [3] Volume 3 Utilization of Hydrogen for Sustainable Energy and Fuels, ed. V. Marcel Van de. 2021, Berlin, Boston: De Gruyter DOI: 10.1515/9783110596274.
- [4] Strategic Research and Innovation Agenda 2021 2027. 2022, Clean Hydrogen JU.
- [5] Kleen G and Padgett E, Durability-adjusted fuel cell system cost. 2020, Reston, VA: SA, Inc.
- [6] Marcinkoski J, Vijayagopal R, Adams J, James B, Kopasz J, Ahluwalia R. DOE Advanced Truck Technologies–Subsection of the Electrified Powertrain Roadmap. Argonne: DOE; 2019.
- [7] Addendum to the Multi Annual Work Plan 2014 2020. 2018, Clean Hydrogen JU.
- [8] Xueqin L, Yan Q, Yudong W, Chao Q, Gang L. A comprehensive review on hybrid power system for PEMFC-HEV: issues and strategies. Energ Conver Manage 2018;171: 1273–91. https://doi.org/10.1016/j.enconman.2018.06.065.
- [9] Das HS, Tan CW, Yatim AHM. Fuel cell hybrid electric vehicles: a review on power conditioning units and topologies. Renew Sustain Energy Rev 2017;76:268–91. https://doi.org/10.1016/j.rser.2017.03.056.
- [10] Chuang S, Jun F, Dong L, Chang J, Ziang G, Beijia L, et al. Energy management strategy based on health state for a PEMFC/Lithium-ion batteries hybrid power system. Energ Conver Manage 2022;271:116330. https://doi.org/10.1016/j. enconman.2022.116330.
- [11] Tsotridis GP, Alberto; De Marco, Giancarlo; Malkow, Thomas, EU harmonised test protocols for PEMFC MEA testing in single cell configuration for automotive applications. 2015.

- [12] Chen H, Song Z, Zhao X, Zhang T, Pei P, Liang C. A review of durability test protocols of the proton exchange membrane fuel cells for vehicle. Appl Energy 2018;224:289–99. https://doi.org/10.1016/j.apenergy.2018.04.050.
- [13] Nguyen HL, Han J, Nguyen XL, Yu S, Goo Y-M, Le DD. Review of the Durability of Polymer Electrolyte Membrane fuel Cell in Long-Term operation: Main Influencing Parameters and Testing Protocols. Energies 2021;14(13). https://doi.org/10.3390/ en14134048
- [14] NREL, DriveCAT Chassis Dynamometer Drive Cycles. 2024, National Renewable Energy Laboratory: http://www.nrel.gov/transportation/drive-cycle-tool.
- [15] Commission E, Vehicle Energy Consumption calculation TOol VECTO. 2019: https://web.jrc.ec.europa.eu/policy-model-inventory/explore/models/model-vecto/.
- [16] Yuan X-Z, Li H, Zhang S, Martin J, Wang H. A review of polymer electrolyte membrane fuel cell durability test protocols. J Power Sources 2011;196(22):9107–16. https:// doi.org/10.1016/j.jpowsour.2011.07.082.
- [17] Yuan X-Z, Zhang S, Sun JC, Wang H. A review of accelerated conditioning for a polymer electrolyte membrane fuel cell. J Power Sources 2011;196(22):9097–106. https://doi.org/10.1016/j.jpowsour.2011.06.098.
- [18] Zhang S, Yuan X, Wang H, Merida W, Zhu H, Shen J, et al. A review of accelerated stress tests of MEA durability in PEM fuel cells. Int J Hydrogen Energy 2009;34(1): 388–404. https://doi.org/10.1016/j.ijhydene.2008.10.012.
- [19] Bae SJ, Kim S-J, Park JJ, Park CW, Lee J-H, Song I, et al. Lifetime prediction of a polymer electrolyte membrane fuel cell via an accelerated startup-shutdown cycle test. Int J Hydrogen Energy 2012;37(12):9775–81. https://doi.org/10.1016/j. iihydene.2012.03.104.
- [20] Jeon Y, Na H, Hwang H, Park J, Hwang H, Shul Y-g. Accelerated life-time test protocols for polymer electrolyte membrane fuel cells operated at high temperature. Int J Hydrogen Energy 2015;40(7):3057–67. https://doi.org/10.1016/j. iihydene.2015.01.010.
- [21] Petrone R, Hissel D, Péra MC, Chamagne D, Gouriveau R. Accelerated stress test procedures for PEM fuel cells under actual load constraints: State-of-art and proposals. Int J Hydrogen Energy 2015;40(36):12489–505. https://doi.org/10.1016/j. iibudeng 2015.07.026
- [22] Nancy G, Thomas B, John K. DOE fuel cell program: Durability technical targets and testing protocols. ECS Trans 2007;11(1):923. https://doi.org/10.1149/1.2781004.
- [23] Ren P, Pei P, Li Y, Wu Z, Chen D, Huang S. Degradation mechanisms of proton exchange membrane fuel cell under typical automotive operating conditions. Prog Energy Combust Sci 2020;80. https://doi.org/10.1016/j.pecs.2020.100859.

- [24] Jeon Y, Sm Juon, Hwang H, Park J, Shul Y-G. Accelerated life-time tests including different load cycling protocols for high temperature polymer electrolyte membrane fuel cells. Electrochim Acta 2014;148:15–25. https://doi.org/10.1016/j. electacta.2014.10.025.
- [25] Mitzel J, Zhang Q, Gazdzicki P, Friedrich KA. Review on mechanisms and recovery procedures for reversible performance losses in polymer electrolyte membrane fuel cells. J Power Sources 2021;488. https://doi.org/10.1016/j.jpowsour.2020.229375.
- [26] Zhang Q, Harms C, Mitzel J, Gazdzicki P, Friedrich KA. The challenges in reliable determination of degradation rates and lifetime in polymer electrolyte membrane fuel cells. Curr Opin Electrochem 2022;31. https://doi.org/10.1016/j. coelec.2021.100863.
- [27] Zhang Q, Schulze M, Gazdzicki P, Friedrich KA. Quantification of effects of performance recovery procedures for polymer electrolyte membrane fuel cells. J Power Sources 2021;512. https://doi.org/10.1016/j.jpowsour.2021.230467.
- [28] Zhang Q, Schulze M, Gazdzicki P, Friedrich KA. Comparison of different performance recovery procedures for polymer electrolyte membrane fuel cells. Appl Energy 2021; 302. https://doi.org/10.1016/j.apenergy.2021.117490.
- [29] Pahon E, Morando S, Petrone R, Péra MC, Hissel D, Yousfi-Steiner N, et al. Long-term tests duration reduction for PEMFC μ-CHP application. Int J Hydrogen Energy 2017;42(2):1527–33. https://doi.org/10.1016/j.ijhydene.2016.06.222.
- [30] Thiele P, Yang Y, Dirkes S, Wick M, Pischinger S. Realistic accelerated stress tests for PEM fuel cells: Test procedure development based on standardized automotive driving cycles. Int J Hydrogen Energy 2024;52:1065–80. https://doi.org/10.1016/j. iihydene 2023 08 292
- [31] Thiele P, Gouveia L, Ulrich O, Yang Y, Liu Y, Wick M, et al. Realistic accelerated stress tests for PEM fuel cells: operation condition dependent load profile optimization. J Power Sources 2024;617. https://doi.org/10.1016/j.jpowsour.2024.234959.
- [32] Colombo E, Casalegno A, Bisello A, Rovatti L, Baricci A. Air-Start-up of PEM fuel Cells under automotive conditions: analysing degradation mechanisms via accelerated protocols comparison. J Electrochem Soc 2025;172(6). https://doi.org/10.1149/ 1945-7111/ade0f1
- [33] Bisello A, Colombo E, Baricci A, Rabissi C, Guetaz L, Gazdzicki P, et al. Mitigated start-up of PEMFC in real automotive conditions: local experimental investigation and development of a new accelerated stress test protocol. J Electrochem Soc 2021;168(5). https://doi.org/10.1149/1945-7111/abf77b.
- [34] Mora D, Colombo E, Casalegno A, Baricci A. Evaluation of PEM fuel cell degradation through accelerated stress tests to investigate heterogeneity of ageing. J Electrochem Soc 2025;172(4). https://doi.org/10.1149/1945-7111/adc62b.
- [35] Colombo E, Baricci A, Mora D, Guetaz L, Casalegno A. An innovative accelerated stress test representative of automotive PEMFC degradation mechanisms validated on

- 1000 hours real-world operation. J Power Sources 2023;580. https://doi.org/10.1016/j.jpowsour.2023.233376.
- [36] Eckhardt P, Henne P, Czarnetzki WT, Wörner R. Simulation and energy management of a fuel cell hybrid heavy-duty truck, in 33rd Electric Vehicle Symposium (EVS33). Oregon: Portland; 2020.
- [37] Bizon N. Real-time optimization strategies of fuel cell hybrid power systems based on load-following control: a new strategy, and a comparative study of topologies and fuel economy obtained. Appl Energy 2019;241:444–60. https://doi.org/10.1016/j. apenergy.2019.03.026.
- [38] Molavi A, Husar A, Hjortberg H, Nilsson N, Kogler M, Monreal JS, et al. State machine-based architecture to control system processes in a hybrid fuel cell electric vehicle. Int J Hydrogen Energy 2023. https://doi.org/10.1016/j. iihydene 2023 07 039
- [39] Zhang H, Li X, Liu X, Yan J. Enhancing fuel cell durability for fuel cell plug-in hybrid electric vehicles through strategic power management. Appl Energy 2019;241:483–90. https://doi.org/10.1016/j.apenergy.2019.02.040.
- [40] Wang Y, Sun Z, Chen Z. Energy management strategy for battery/supercapacitor/fuel cell hybrid source vehicles based on finite state machine. Appl Energy 2019;254. https://doi.org/10.1016/j.apenergy.2019.113707.
- [41] Torreglosa JP, Garcia-Triviño P, Vera D, López-García DA. Analyzing the improvements of energy management systems for hybrid electric vehicles using a systematic literature review: how far are these controls from rule-based controls used in commercial vehicles? Appl Sci 2020;10(23). https://doi.org/10.3390/ appl0238744.
- [42] White FM, Fluid Mechanics. 2011: McGraw Hill.
- [43] Erickson RW, DC-DC Power Converters. 2007: John Wiley & Sons Ltd DOI: https://doi.org/10.1002/047134608X.W5808.pub2.
- [44] Frano B, Chapter Nine Fuel Cell System Design, in PEM Fuel Cells (Second Edition), B. Frano, Editor. 2013, Academic Press: Boston. p. 305-372.
- [45] Sundström O, Stefanopoulou A. Optimum battery size for fuel cell hybrid electric vehicle—part I. J Fuel Cell Sci Technol 2006;4(2):167–75. https://doi.org/ 10.1115/1.2713775.
- [46] Piela P, Mitzel J, Rosini S, Tokarz W, Valle F, Pilenga A, et al. Looking inside polymer electrolyte membrane fuel cell stack using tailored electrochemical methods. J Electrochem Energy Convers Storage 2020;17(3). https://doi.org/10.1115/ 1.4046106.
- [47] Pei P, Chang Q, Tang T. A quick evaluating method for automotive fuel cell lifetime. Int J Hydrogen Energy 2008;33(14):3829–36. https://doi.org/10.1016/j. ijhydene.2008.04.048.
- [48] Frano B. Chapter Seven Fuel Cell Modeling. In: Frano B, editor. PEM Fuel Cells (Second Edition). Boston: Academic Press; 2013, p. 217–63.